Chapter 7. Optical Effects Induced by Pulse Gamma-Neutron Irradiation

7.1. Main Problem

Practically all elementary excitations, such as electrons, holes, excitons, phonons, plasmons etc. arise in dielectrics irradiated with a γ-neutron pulse. The occurrence and relaxation of the elementary excitations in transparent dielectrics is accompanied by radiation-induced optical effects (RIOE).

The external RIOE manifestations, such as radiation-induced luminescence and spectrum transmission variations can be detected by means of fast spectrophotometry. The qualitative estimation of the external RIOE manifestations permits a speedy and effective selection of the studied dielectrics according to levels of optical radiation hardness and, finally, determination of their applicability under particular irradiation conditions. Here, electromagnetic calorimeters for a new generation of accelerators are implied.

The information about RIOE, obtained by fast spectrophotometry techniques, is of primary interest for development of physical models of the processes which occur in dielectrics exposed to a γ-neutron pulse. This technique permits detection, and, in some cases, assessment of the influence on the radiation hardness of uncontrolled impurity and intrinsic defect centres incorporated into the crystal in the course of the synthesis. As a rule, since the concentrations of such defects are insignificant, they cannot be detected by conventional control techniques, namely, measurements of the postirradiation absorption, accurate spectrophotometry etc.

The commonly used technique of assessment of radiation hardness of dielectrics is based on comparison of the transmission spectra before and after irradiation. They characterize only part of the process of defect formation in which the defects have long-term relaxation periods. *The results obtained cannot serve as a database on radiation hardness, because, in principle, they do not comprise the total information on the response of the irradiated medium. They permit detection of the formed optical absorption centres in the dielectric and their concentration at the moment of measurement. As the measurements are made only within some time after irradiation, only the RIOE which are quite stable with the time are detected.*

Such centres are being formed simultaneously with the processes of thermo- or radiation-induced destruction of these (stable) and other (unstable) optical centres. This information cannot be obtained using conventional techniques of studying radiation hardness. Nevertheless, this can be an important component of the actual scintillator response to irradiation.

A remarkable drawback of commonly used techniques of studying radiation hardness of dielectrics is the inconsistency between the employed conventional radiation sources (in the compositions and energies) and the radiation fields under actual operation conditions for scintillators. The radiation fields created by a γ-neutron pulse source of electromagnetic radiation within a wide range of energies provide better models of operation conditions for scintillators in EM-calorimeters. The complex composition of the pulse radiation which is advantageous at the search stage, requires separation of γ- and neutron components during more detailed studies of selected materials.

Along with the above merits of the fast spectrophotometry, combined with the pulse radiation, this technique possesses essential disadvantages. First, the experiment is quite tedious and, second, it is quite difficult to provide the shielding of the detection systems. That is why this technique cannot be applied for characterization of a vast number of materials at the stage of preliminary search which is considered in this book. This technique can be profitable for characterization of a limited number of scintillators after they have been selected on the basis of research studies that comprise determination of radiation hardness by conventional proximate techniques.

7.2. Experimental Methods

The above ideas were used for elaboration of a fast spectrophotometer equipped with a digital detection system and software for processing experimental data. The flow-chart of the experimental unit is shown in Fig. 7.1. This unit comprises a source of light (1) located together with the spectrophotometer behind the shielding (2). The area exposed to the γ-neutron pulse contains the sample (3) and the detector (5) that detects the amplitude-time distribution of the intensity of the effect of the total flux $\Phi_{\Sigma(\gamma\text{-}n)}(t)$ and, separately, those of the γ-, $\Phi_\gamma(t)$, and neutron, $\Phi_n(t)$, components.

The flux of light I_o which probes the studied sample before, during and after the action of the neutron pulse is taken as a standard in the form of spectrum-time distribution of the intensities $I_o(\lambda, t)$. The flux of light that has passed through the sample during irradiation and afterwards carries the information about the external RIOE manifestations, excited in the sample. The flux passes the information over to the spectrophotometer.

The fast spectrophotometer (4) [7.1] has two identical detection channels and provides for detection of spectra with frequencies $5x10^4$ sec^{-1} within the 0.25 - 1.50 μm band. Removable profiled diffraction lattices with 600 dashes/mm are used as dispersion elements. The Relay criterion for the 577/579 nm mercury doublet is fulfilled.

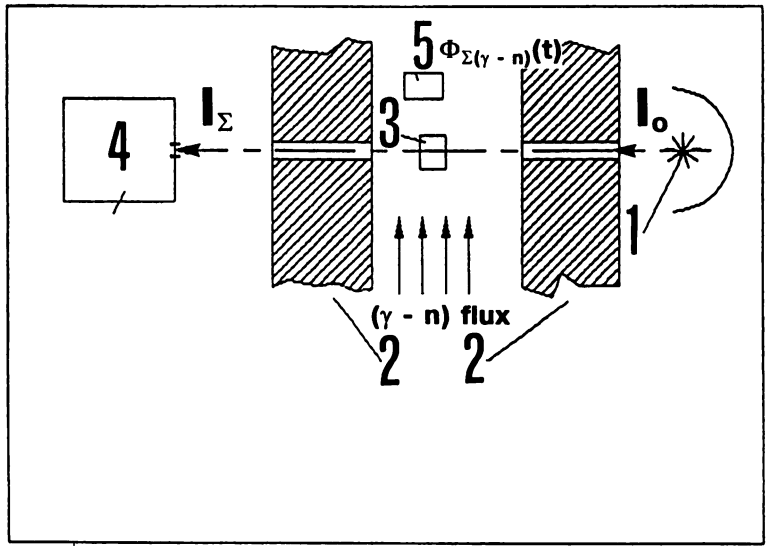

Fig. 7.1 Flow-chart of the experimental set-up

The amplitude-time distribution of the total intensity of the γ-neutron effect has a nonsymmetric, with respect to the extremum, bell-like shape. The halfwidth $\Phi_{\Sigma(\gamma+n)}(t)$ (below, for brevity, we shall denote this function as $\Phi(t)$) varies within the range ± 100 μs, the effective time of the action is 500 μs, the intensity averaged over the energies can be estimated as 10^8 p/sec within 100 μs from the position of the maximum $\Phi(t)$ on the time axis. The equipment for generation of γ-neutron pulses is described in [7.2].

The information array was formed in the course of the experimental studies as follows: before the action of the radiation pulse the graduation linear spectra had been recorded so as to fill the certain part of the spectrum chosen in advance. Gas-charge chambers (mercury and cadmium) with their known line spectra were used. Then, the source of light, namely a quartz halogen incandescent lamp, was mounted. Upon insertion of the sample, the standard intensity distribution $I_i(\lambda, t)$ was detected at $\Phi(t) = 0$ of the flux of light passed through the sample within the chosen range of wavelengths.

Under irradiation, the sequence of scans within the set spectrum range as well as the amplitude-time distribution $\Phi(t)$ were recorded. The output data array from the digital detection equipment were ordered in wavelengths and times and served as the basis for the graphic interpretation (three-dimensional picture) of the total array of radiation doped RIOE in the sample.

The three-dimensional picture of the RIOE complex in the coordinates of wavelengths (λ), amplitude (η) and time (t) is a vivid representation of the matrix $A = [\eta_{ik}]$, in which each element $I_{ik} = \eta(\lambda_i, t_k)$ is calculated as the relation $I(\lambda_i, t_k)/I_o(\lambda_i, t_k)|_{\Phi(t) = 0}$, where λ_i and t_k are chosen, respectively, within the scanned wavelength band and in the section of the time axis where $\Phi(t)$ differs from zero. Apparently, $\eta(\lambda, t)$ varies within the range $\eta_{max} > 1 > \eta_{min}$. At the stage of preliminary analysis the band ($\eta_{max} - 1$) and ($1 - \eta_{min}$) can be interpreted as spectrum - time ranges of luminescence or variations of the spectrum transmission, respectively.

During a detailed analysis of the RIOE complex in order to build mathematical models of the physical processes that make up the complex itself, the full matrix $\eta[i, k]$ should be applied. The matrix $\eta[i, k]$ is supplemented by the line (i + 1) that contains a discrete distribution of $\Phi(t)$ and the column (k + 1) that is the frequency calibration of the scanned range $1024 \times 0.5 = 512$ μsec. In our case the matrix contained 1024 + 1 columns with the time step 0.5 sec and 80 + 1 line. The wavelength digitization is not a constant and depends on the chosen limits. All the three-dimensional pictures of RIOE reported in this book were obtained under similar conditions for the time interval $1024 \times 0.5 = 512$ μsec. The three-dimensional RIOE pictures are conditionally limited by parts of the unit plane $\eta(\lambda, t) = 1$ along the time axis.

As an example which illustrates the power of the suggested technique we shall consider the data on the well known crystals of pure and Nd^{3+}-doped ytrium - aluminium garnet (YAG), Fig. 7.2. Uncontrolled impurity and intrinsic (lattice) defect centres are manifested in the form of luminescence peaks, distributed rather evenly within the scan wavelength band. The positions of the extrema on the time axis indicate two different groups of centres. They are detected on the projections of their time dependencies, which represent the sum $\eta(t)|_{\lambda = const}$ shown in the right-hand part in Fig. 7.2.

One group which comprises 4 - 5 extrema, which coincide with the maximum of $\Phi(t)$ is, apparently, due to an uncontrolled Nd^{3+} activator, of a very small concentration. The group of extrema, made up of 11 - 13 peaks, is located on the time axis in the range that corresponds not to the maximum Φ (t), but to the position of the maximum $d\Phi(t)/dt$. This difference is not

accidental, and it evidences that there are certain features, according to which the defects are united into two groups. Each group has intrinsic kinetic distinctive features in the general RIOE picture. During a detailed analysis of the found group of centres an appropriate defect centre can be assigned to each extremum proceeding from the spectroscopic manifestations with an allowance for the distribution of the extrema within the frequency band λ on the time axis **t**. The complex character of radiation can be the reason for the occurrence of multiple active centres. Such a detailed analysis was not the goal of our experimental study. A compact interpretation of the full representation of the matrix $\eta(\lambda, t)$ is shown in Fig. 7.2. The scale step $\Delta t \sim 12$ μsec was chosen on the time axis. The compact form of representation is convenient for a qualitative analysis of the general RIOE picture under irradiation. Sometimes it may lead to erroneous conclusions, however.

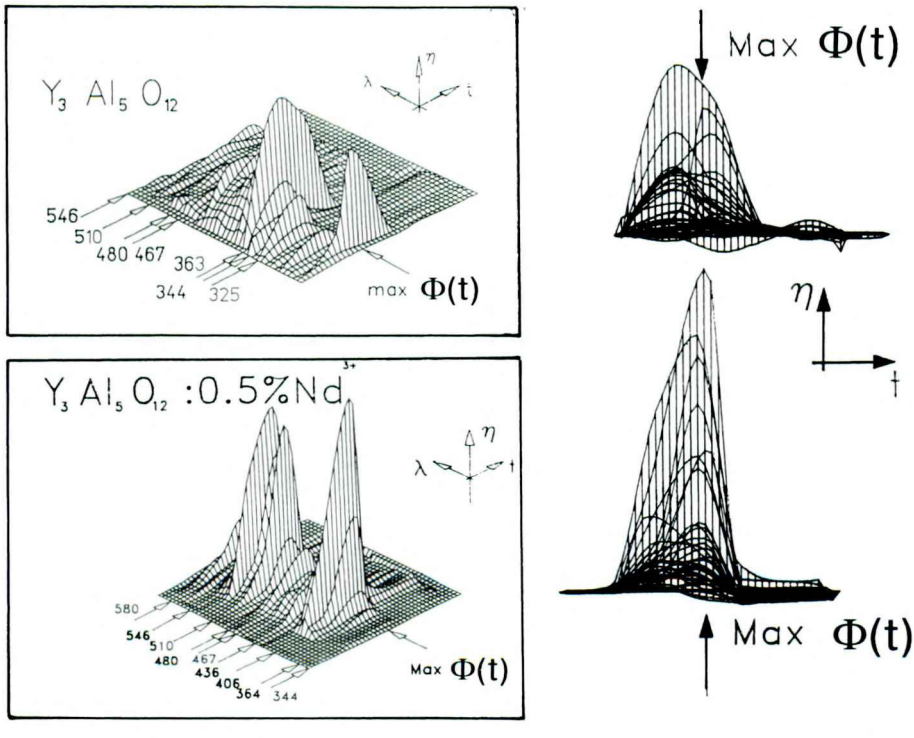

Fig. 7.2. Graphic interpretation of a RIOE complex, stimulated in a YAG-matrix (top), YAG:Nd^{3+}(bottom), supplemented by the sum of projections $\eta(t)|_{\lambda = const}$

As an example, let us consider the most intensive peak in the RIOE picture for the crystalline matrix of YAG, Fig. 7.2, with a maximum for the

wavelength ≅ 370 nm. In this Figure the sum of projections $\Sigma\eta(t)|_{\lambda=const}$ is shown on the right in a compact form, this extremum can be interpreted as a time convolution of two peaks. If we take the full matrix of the values $\eta(\lambda, t)$ the extremum will split into two distinctive spectrum resolved luminescent peaks. This shows how carefully the analysis of general RIOE pictures should be made.

7.3. Objects of Studies

Studies of RIOE in single crystals of metal fluorides were performed for a few compositions, as the experiments were quite tedious. The well known scintillators BaF_2 and CeF_3 from the family of single component fluorides were studied. Multicomponent fluoride materials were represented by heterovalent solid solutions $Ba_{1-x}Ce_xF_{2+x}$ with the fluorite type structure which are formed in the same system BaF_2 - CeF_3, as well as nonstoichiometric crystals $Cd_{0.97}Ce_{0.03}F_{2.03}$, $Cd_{0.98}Ce_{0.01}La_{0.01}F_{2.02}$ and $Ba_{0.882}Gd_{0.118}F_{2.118}$. All the multicomponent crystals, as well as CeF_3, were obtained using the technique in which an active fluorinating atmosphere is employed during crystallization. BaF_2 crystals were obtained using this and industrial (vacuum) technology, see Chapter 5.

7.4. Experimental Results

Fig. 7.3 presents results of the studies performed using the above technique for the three materials formed in the same system BaF_2 - CeF_3. There are two effects that are responsible for the formation of the surface $\eta(\lambda, t)$, namely, luminescent radiation and increment of optical density.

In a BaF_2 crystal, obtained in a fluorinating atmosphere, the effect of luminescent radiation is predominant, see Fig. 7.3 a. It is represented by a peak with a complex (in the wavelengths) profile, whose extremum coincides with the maximum of the effect of $\Phi(t)$ on the time axis. Without identifying luminescence mechanisms that are responsible for that peak, we note that intrinsic (excitonic) luminescence of BaF_2 is observed in this band. An insignificant increment of optical density is detected only in the ≅ 470 nm band. This confirms the data on a sufficiently high radiation stability of BaF_2 crystals (see Table VI.6.). In CeF_3 crystals (Fig. 7.3 c) the peak of luminescence radiation that coincides with the maximum of the effect of $\Phi(t)$ also has a complex profile λ and it is widely distributed over the spectrum. At the same time, a significant increment of the optical density in the 350 - 500 nm band is quite distinct. This finding contradicts the data on a high radiation hardness of CeF_3 obtained by various authors. It is not consistent with the results of our own measurements made on CeF_3 crystals irradiated by

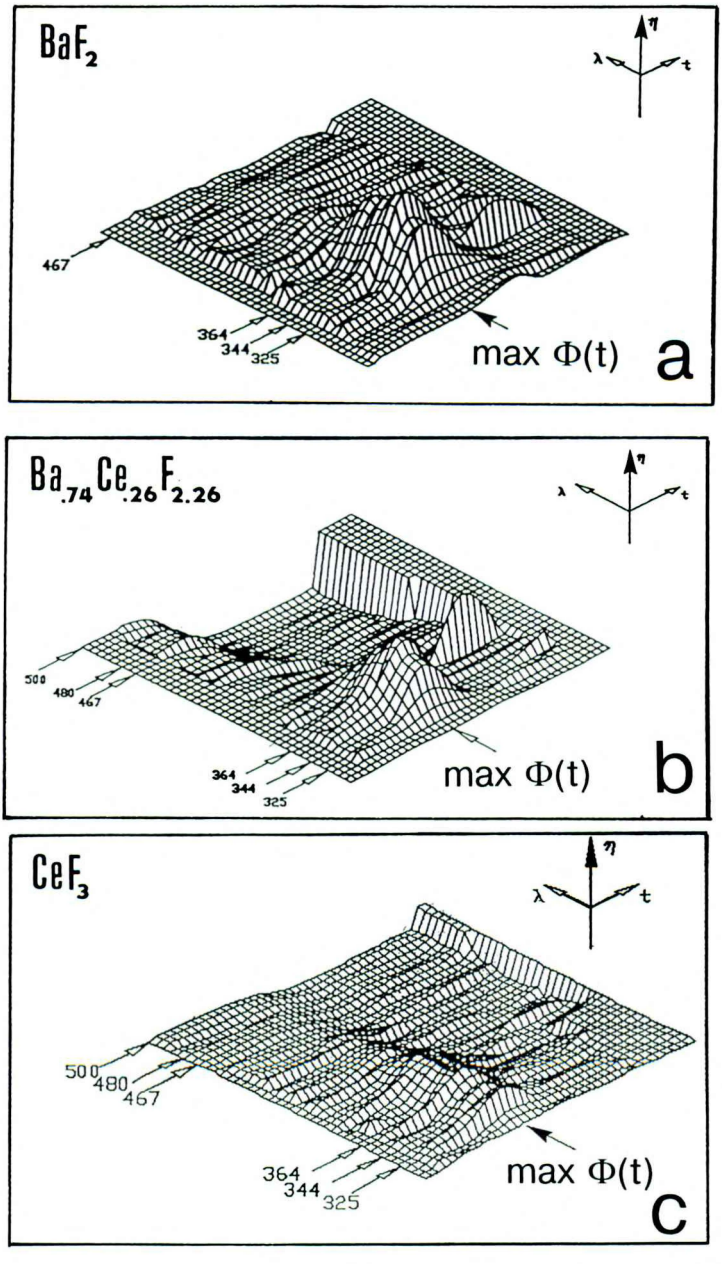

Fig. 7.3. Graphic interpretation of a RIOE complex, stimulated in BaF_2, $Ba_{0.74}Ce_{0.26}F_{2.26}$ and CeF_3

stationary radiation sources (see Chapter 6). Further experimental studies are required in order to find the reasons for such inconsistency. As this technique is rather specific, there may be several such reasons, including fast quenching of the formed centres of optical absorption.

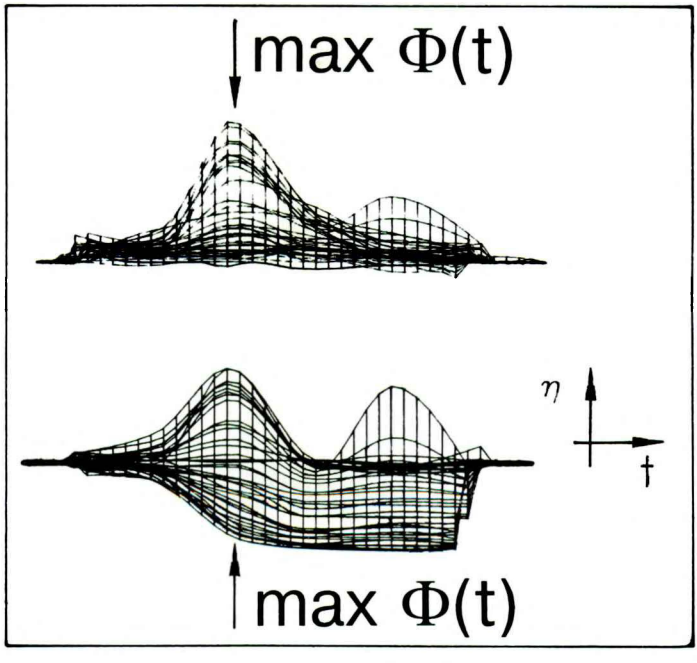

Fig. 7.4. Sum of amplitude-time projections for BaF_2 (top) and $Ba_{0.74}Ce_{0.26}F_{2.26}$

For a $Ba_{0.74}Ce_{0.26}F_{2.26}$ crystal, isostructural with BaF_2, the RIOE picture shows distinctly a radioluminescent peak with a complicated profile in the 300 - 800 nm band, that coincides in time with the maximum of $\Phi(t)$. Absorption increment prevails in the 400 - 500 nm band. This correlates with a low radiation hardness found for these crystals in Chapter 6. In the RIOE picture for these crystals, similar to the case of BaF_2, quite narrow in λ, but intensive luminescence peaks which are 160 - 200 μs delayed with respect to the maximum of the effect of $\Phi(t)$, were detected. The delay times for this peak are the same for both crystals, as is seen from the sections projected onto the amplitude - time plane, Fig. 7.4. At the same time, the position of the intensity maximum differs in the wavelengths for both crystals. In $Ba_{0.74}Ce_{0.26}F_{2.26}$ the maximum coincides with the luminescence wavelength of pure CeF_3, according to [7.3.] (photoexcitation).

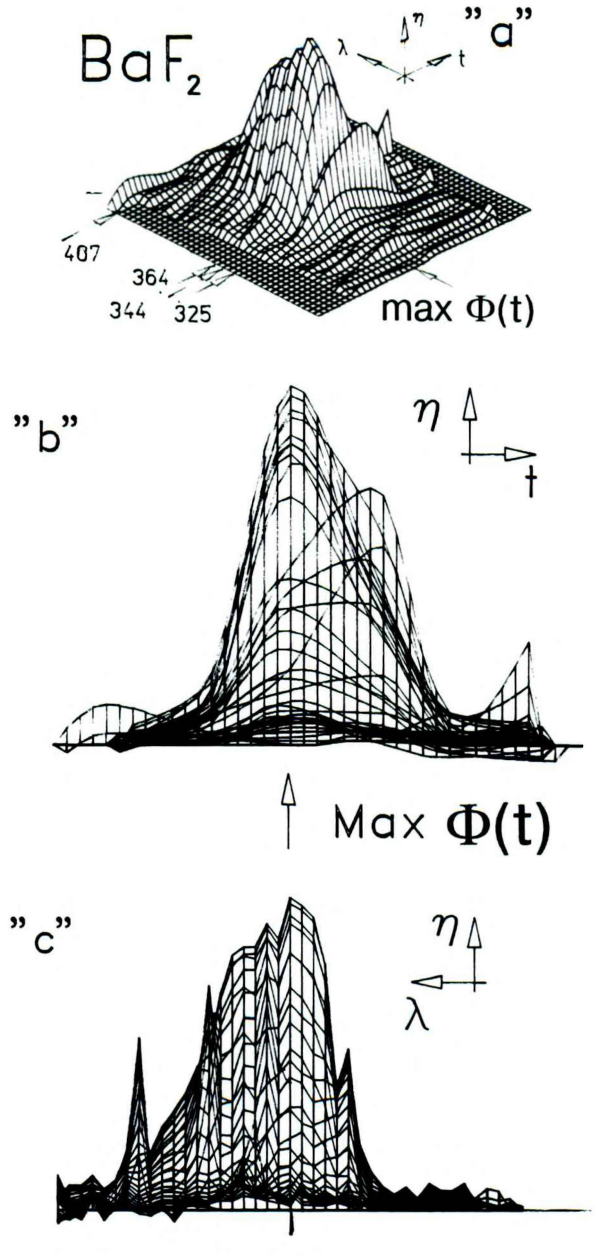

Fig. 7.5. Graphic interpretation of a RIOE complex, stimulated in a BaF_2 crystal obtained using "vacuum" technique (a), sum of amptitude-time projections (b), sum of amplitude-wavelength projections (c)

It is rather difficult to assess without additional studies what possible mechanism of relaxation of elementary excitations in dielectrics can be responsible for that effect. The reason may be a burst of γ- and β- radiation excited by nucleus active component of the radiation pulse in the sample (see Chapter 6) and in the surrounding parts of the unit. The delay component may also be due to re-emission of the absorbed energy which is accumulated by the formed defect centres in the form of a photon beam, rather narrow in the range. The observed time shift is needed particularly for accumulation of the defect centres in sufficient concentrations.

In order to confirm the reproducibility of the effect of "delayed" luminescence which can play an important role in the total response of the detection system to irradiation, BaF_2 crystals obtained using vacuum technology were studied. The results are shown in Fig. 7.5. BaF_2 crystals obtained using different technologies, differ significantly. The crystals obtained using the vacuum technology, have a more complex composition with a better resolution of the spectrum wavelengths, Fig. 7.5 c. The luminescence response of these crystals also exhibits two groups of defects that differ in the maximum intensities of the impact pulse with respect to time, Fig. 7.5 a, b. In other words, the effect of luminescence radiation delay is observed as well in crystals obtained by other manufacturers using other technologies.

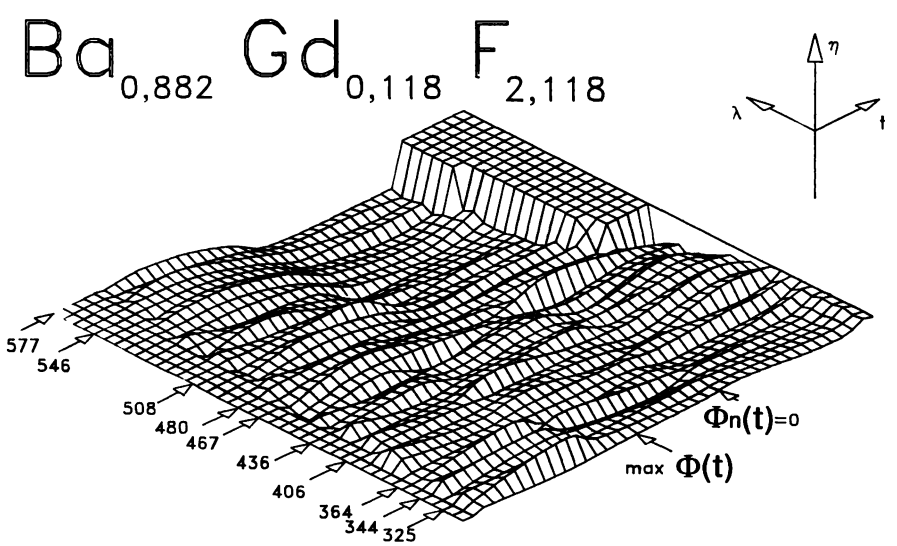

Fig. 7.6. Graphic interpretation of a RIOE complex, stimulated in $Ba_{0.882}$ $Gd_{0.118}$ $F_{2.118}$

In $Ba_{0.882}Gd_{0.118}F_{2.118}$ crystals, as Fig. 7.6 shows, absorption increment effects prevail within the entire studied spectrum range. The high absorption is most evident within the ≅ 500 - 577 nm band. Under stationary conditions these crystals exhibited low radiation hardnesses as well and, therefore, they were not included into Table VI.6.

Among all of the crystals in which a complication of their chemical composition was accompanied by a more remarkable increase in the radiation hardness, according to data from post-irradiation measurements, we chose CdF_2. Nominally pure single crystals, as is seen from Table VI.6 possess a low radiation hardness in the stationary radiation fields. The incorporation of cerium is accompanied by a several-fold increase in the radiation hardness. The RIOE picture for γ-neutron irradiated $Cd_{0.97}Ce_{0.03}F_{2.03}$ crystals is shown in Fig. 7.7 a. The effect of radiation-induced luminescence with a maximum in the vicinity of 370 nm is predominant. The effects of the largest increment of the optical density in narrow spectrum ranges vanish quite quickly with time. These data fully coincide with the record values of radiation hardness of these crystals, reported in Chapter 6.

The effect of a further complication of the chemical composition of crystals due to isomorphic incorporation of small lanthanum and Ce^{3+} contents into the crystalline lattice, is shown in Fig. 7.7 b. Despite the low La^{3+} content, luminescence at 370 nm is completely quenched. The level of spectrum - time excitations in this crystal is low, which is seen on the amplitude - time projections, shown in Fig. 7.7 c. These data correlate with the data on a high radiation hardness of $Cd_{0.98}La_{0.01}Ce_{0.01}F_{2.02}$ single crystals. At the same time, they exhibit an effective influence of small amounts of dopants on the spectrum composition of the radioluminescence response of the irradiated optical medium. The effect of luminescence quenching within the entire wavelength band (325 - 580 nm) is particularly evident on the projections of $\eta(\lambda)|_{t = const}$, shown in Fig. 7.7 d. Similar effects, presented in Table VI.6 for stationary radiation fluxes, did not carry information about changes in spectrum compositions of luminescence, because of the techniques used.

7.5. Discussion

The first studies of RIOE in multicomponent fluoride crystals with the fluorite structure $M_{1-x}R_xF_{2+x}$ $(0.1 < x < 0.3)$ inside the channel of the γ-source unit were carried out in [7.4, 5]. They showed that the γ-^{60}Co radiation brings about a burst of luminescence which passes through the maximum within the first few seconds and attains saturation. In [7.4], quenching of the "intrinsic" (excitonic) component of luminescence was first noted in MF_2 with M = Ca, Sr, Ba upon isomorphic substitutions of M^{2+} by

all RE ions in these crystalline matrices. This effect was later observed in barium fluoride [7.6 - 8],etc. For these fluorides the maxima in the intensity of this component are at 280, 300 and 310 nm, accordingly. We shall be concerned with the data on γ-luminescence of $Ba_{0.71}Ce_{0.29}F_{2.29}$ crystals, for which a wide luminescence band with a maximum 360 nm was observed in [7.4].

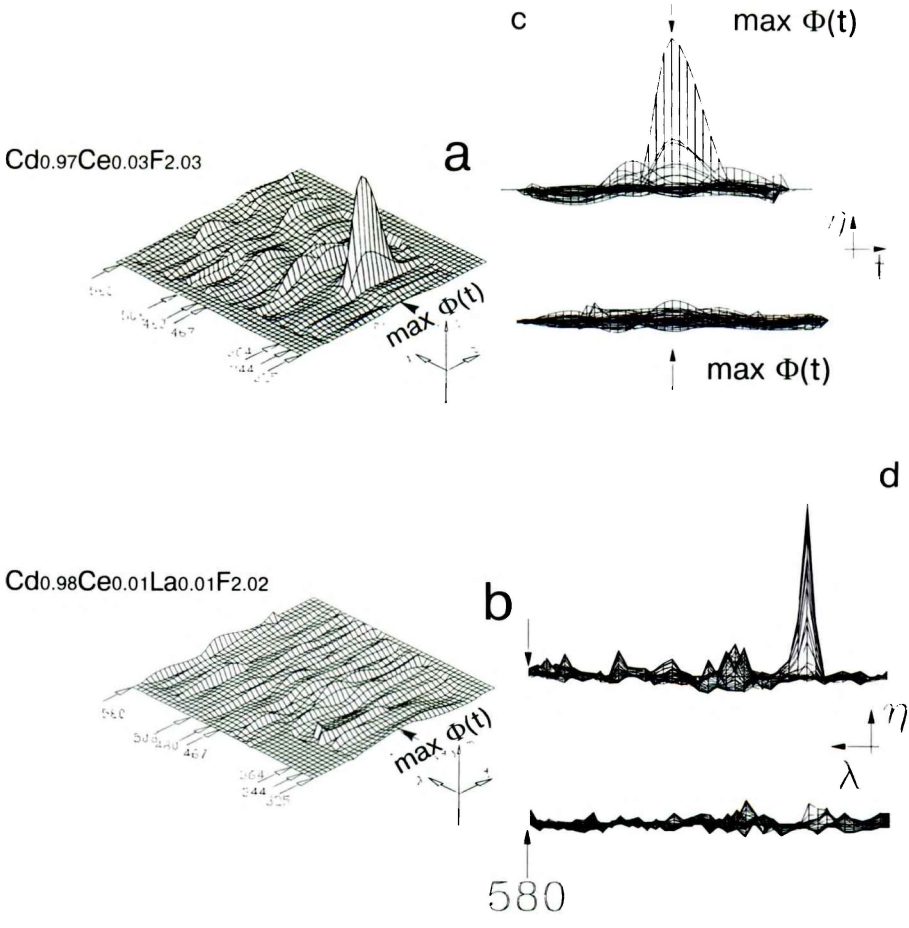

Fig. 7.7. Graphic interpretation of a RIOE complex, stimulated in $Cd_{0.97}Ce_{0.03}F_{2.03}$ (a), $Cd_{0.98}Ce_{0.01}La_{0.01}F_{2.02}$ (b), supplemented accordingly by sums of amplitude-time projections (c), and amplitude - λ-projections (d) for both compositions of the crystals

The obtained data on RIOE upon γ-neutron radiation, Fig. 7.4 b, qualitatively agree with these observations. At the same time, the authors of [7.4, 5] noted, as well as we did, that the spectrum compositions of strongly and weakly cerium doped $Ba_{1-x}Ce_xF_{2+x}$ crystals differed. Recently, the authors of [7.9] have investigated variations of radioluminescence regions of $Ba_{1-x}Ce_xF_{2+x}$ crystals with an increase in the CeF_3 content from 0.001 to 4.9 mole %. The resultant region has a maximum of ~ 360 nm for the sample with the maximum cerium content. This effect occurs, in the authors` opinion, due to small oxygen impurities that form Ce^{3+} - O^{2-} centres in the crystal. In our $Ba_{0.74}Ce_{0.26}F_{2.26}$ crystals, similar to the case described in [7.4, 5], oxygen impurities were removed from the starting reagents to a highest possible extent. The crystals were grown under the conditions excluding pyrohydrolysis. That is why in order to explain changes in the spectra of γ-luminescence of concentrated $Ba_{1-x}Ce_xF_{2+x}$ solid solutions (against weakly doped) other reasons should be sought.

There is an evident difference between the conclusions about the high radiation hardness of $Ba_{1-x}Ce_xF_{2+x}$ crystals reported in the papers [7.4, 5], (x = 0.29), as well as in our study (see Chapter 6), and the data about a strong absorption within a wide spectrum range under the effect of a γ-neutron pulse, Fig. 7.3. A possible explanation was suggested in [7.5], where the low thermal stability of coloration centres in $M_{1-x}R_xF_{2+x}$ crystals with some RE, including Ce, was reported. *A fast "annealing" of the defects that give rise to induced absorption, can lead to erroneous conclusions in postirradiation studies of radiation hardnesses of materials.*

We could mention other distinctions between the RIOE observations made by the fast spectrophotometry technique, and conventional techniques. Anyway, they are quite evident. In some cases, including the case considered in this chapter, they are of a principal character.

The described approach can be employed for modeling the radiation optical effects that occur in the course of an EM shower. Our estimations have shown that the materials are exposed to irradiation with the dose rates 10^5 - 10^7 rad/sec in the trunk of an EM shower at high energies of the accelerated particles planned at LHC, SSC, etc. devices within short times of its development (several nsec). The duration of the used γ-neutron pulses prevents observation of RIOE within times from several nanoseconds to 200 μsec. The presence of neutrons in the pulses which are absent in an EM shower complicates the interpretation of the results obtained.

Thus, the fast spectrophotometry technique for RIOE studies under irradiation is more informative than conventional post-irradiation studies of radiation damages. Particularly important information can be obtained for the case of the radiation damages that have low stabilities and that are relaxed within the first few minutes or hours after the radiation ceases. The

interpretation of the graphic image of a RIOE complex in the fast spectrophotometry technique is quite complicated and requires employment of other techniques of spectroscopic studies. It is evident, however, that this technique should be included into comprehensive characterization of the scintillators that were chosen at the preliminary stage of search.

REFERENCES

7.1. Vasin E.N., Motin Yu.D., Device for fast spectral scanning, Patent 1245896, 22 March 1986 g., Bulletin Izobretatelia, 1986, No. 27, 131 (in Russian).

7.2. Windsor K., Neutron diffusion from pulse source, Ed. "Energoatomizdat", Moscow: 1985, 78 - 82, 143 - 150 (translated from English).

7.3. Kobayashi M., Ishii M., Krivandina E.A., Litvinov M.M., Peresypkin A.I., Prokoshkin Yu.D., Rykalin V.I., Sobolev B.P., Takamatsu K., Vasilchenko V.G., Cerium fluoride, a highly radiation-resistive scintillator, Nucl. Instrum. Meth., 1991, v. A302, 443 - 446.

7.4. Vachidov Sh.A., Tavshunskii G.A., Rustamov Ja., Bessonova T.S., Sobolev B.P., Fedorov P.P., Nuclear radiations action on multicomponent fluorides, Zhurn. Techn. Fisiki, 1979, v. 49, No. 9, 1943 - 1949 (in Russian).

7.5. Rustamov Ja., Tavshunskii G.A., Khabibullaev P.K., Bessonova T.S., Sobolev B.P., The radiation coloring of nonstoichiometric $M_{1-x}R_xF_{2+x}$ crystals with defect fluorite structure, Zhurn. Techn. Fisiki, 1985, v. 55, No. 6, 1150 - 1158 (in Russian).

7.6. Golovin A.V., Melchakov E.N., Michailin V.V., Rodnyi P.A., Excitonic and core-valency radiative transitions in single crystals BaF_2 - LaF_3, Fisika Tverdogo Tela, 1989, v. 31, No. 4, 253 - 256 (in Russian).

7.7. Woody C.L., Levy P.W., Kierstead J.A., Slow component suppression and radiation damage in doped BaF_2 crystals, IEEE Trans. Nucl. Sci., 1989, v. 36, No. 1, 536 - 542.

7.8. Schotanus P., Van Eijk C.W.E., Hollander P.W., Pijpelink J., Development study of a new gamma camera, IEEE Trans.Nucl.Sci., 1987, NS-34, No.1, p.272 - 276.

7.9. Visser R., Andriessen J., Dorenbos P., van Eijk C.W.E., Energy transfer and energy levels in BaF_2:Ce, International Workshop "Crystal 2000", Chamonix, September 22 - 26, 1992, France, Proceedings, 201 - 206.